Rate Dependence of Flexural Tensile Strength of Laurentian Granite

F. Dai & K. Xia
University of Toronto, Toronto, Canada

ABSTRACT: Due to difficulties associated with gripping in direct tension, indirect methods are commonly used to measure rock tensile strength. In this work, we adopt an innovative indirect tensile test method: Semi-Circular Bend (SCB) to measure the tensile/flexural strength of Laurentian granite (LG). The static tests are carried out with a servo-controlled material testing machine and the dynamic tests are conduced with a Split Hopkinson Pressure Bar (SHPB) system. Pulse shaping technique is adopted to achieve dynamic force equilibrium in SHPB to facilitate data regression. Finite element method is used to relate the failure load to the tensile strength. Strong rate dependence of the tensile strength is observed. The flexural strength is higher than the tensile strength measured using Brazilian Disc (BD). This difference is rationalized using the non-local theory. To further validate the method, a coupled Finite element/Discrete element method (Fem/Dem) in conjunction with the smeared crack model is utilized to simulate the fracture process during dynamic SCB tests. The resulting fracture patterns are qualitatively consistent with those from recovered samples. Both the experimental and numerical methods have validated the results and this new method is readily to be used for other rocks and other brittle materials.

1 INSTRUCTION

Rocks are considerably weaker in tension than in compression. Characterizing tensile strength of rocks thus is of great importance in many engineering and geophysical applications. Tensile strength is defined as the failure stress of a cylindrical rock specimen in a pure uniaxial tensile loading. Thus, direct pull test appears to be best suited for tensile strength measurement. However in practice, the ideal uniform stress state in the specimen is rarely provided. Premature failure can be generated due to stress concentration around grips as well as bending effects due to instrumental misalignments. Because of these difficulties associated with experimentation in direct tensile tests, various of indirect methods have been proposed as convenient alternatives to measure the tensile strength of rocks; some examples are Brazilian disc test (Bieniawski & Hawkes, 1978; Coviello et al., 2005; Hudson et al., 1972; Mellor & Hawkes, 1971), ring test (Coviello et al., 2005; Hudson, 1969; Hudson et al., 1972; Mellor & Hawkes, 1971), and bending test (Coviello et al., 2005). These indirect methods aim at generating tensile stress in the sample by far-field compression, which is much easier and cheaper in instrumentation than direct pull tests.

Existing attempts to measure rock tensile strength are mostly limited to quasi-static loading, primarily due to the difficulties in the dynamic experimentation and subsequent data interpretation. However, in many mining and civil engineering applications, such as quarrying, rock cutting, drilling, tunneling, rock blasts, and rock bursts, rocks are stressed dynamically. Accurate characterizations of rock tensile strength over a wide range of loading rates are thus crucial. Due to the reasons discussed above for static tension tests, few direct dynamic tensile tests have been

attempted (Goldsmith et al., 1976), and research efforts have concentrated on extending the indirect methods from quasi-static to dynamic loading. Zhao and Li (Zhao & Li, 2000) measured the dynamic tensile properties of granite with the Brazilian disk and three point bending techniques; the loading was driven by air and oil and thus had a limited loading rate range. To attain tensile strength of rocks under high loading rates, most researchers used the standard dynamic testing facility, split Hopkinson pressure bar (SHPB). For examples, conventional SHPB tests were conducted on Brazilian disk and flattened Brazilian disk specimens of marble (Wang et al., 2006) and on Brazilian disk specimens of argillite (Cai et al., 2007) to measure their dynamic tensile strengths. Quasi-static analysis has been used in these works to relate far-field peak load to the tensile strength of the sample without sufficient justification. It is well known that in the dynamic tests featuring high loading rates, the induced stress in the sample is transient, which leads to loading inertia effect. To use quasi-static analysis, one must take this inertia effect into account for accurate data reduction.

Recently, we proposed an indirect tensile test method- semi-circular bend (SCB) to measure the dynamic flexural tensile strength of rocks and other brittle solids (Dai et al., 2008). We demonstrated that sizeable inertial effects are inevitable in a conventional dynamic SHPB test. The inertial effect has not been taken into account in previous attempts of measuring rock tensile strength using SHPB (Cai et al., 2007; Wang et al., 2006). In our proposed SCB-SHPB method, we modified the loading pulse using a pulse shaping technique. With the carefully shaped loading pulse, we showed that the dynamic force balance can be achieved throughout the dynamic loading period. We also demonstrated that with dynamic force balance, the stress history at the specimen failure spot deduced from quasi-static finite element analysis agrees with that deduced from full dynamic finite element analysis. In addition, the failure time detected with strain gauge on the sample coincides with the peak of the far-field load. We thus concluded that the loading inertial effect was minimized and quasi-static stress analysis of the sample was valid despite of the dynamic loading with the dynamic force balance (Dai et al., 2008). This method thus provides an easy and cost-efficient way of determining the dynamic tensile strength of rock-like brittle solids.

Following our proposed and SCB-SHPB method, we systematically measure the flexural tensile strength of Laurentian granite (LG) in this work. Static measurement is conducted with a servo-controlled material testing machine and the dynamic experiment is carried out with a 25 mm SHPB system. SCB is chosen for this study, not only because it is core-based, but also because it favors dynamic force balance with its shorter dimension along the loading axis as compared to a full disc. It is commonly believed that it takes the stress wave to travel in the sample for several rounds before the stress reaches an equilibrium state in SHPB tests (Ravichandran & Subhash, 1994). Shorter samples thus facilitate the dynamic force balance. The pulse shaping technique (Frew et al., 2001, 2002) is used to achieve dynamic force balance and thus reduce the loading inertial effect. Momentum-trap technique is employed to achieve single-pulse loading so as to relate the failure pattern to a well-defined loading pulse. A combined finite-discrete element method (FEM/DEM) (Munjiza et al., 1999) is used to simulate the dynamic SCB test. The fracture pattern obtained from numerical simulation agrees with that from recovered specimen. This agreement demonstrates the nature of tensile failure of the specimen in SCB-SHPB tests. Rate dependence of the flexural tensile strength of LG is observed. The dynamic flexural tensile strength is consistently higher than the dynamic tensile strength for the same rock (Zhao & Li, 2000). This difference is interpreted using a non-local failure approach (Carter, 1992; Van de Steen & Vervoort, 2001).

2 EXPERIMENTAL SETUP

Static measurement is conducted with an MTS hydraulic servo-control testing system (Fig.1a). TestingSart-II (digital controller) is used to control the testing process and MTS TestingWare-SX software is utilized to set the testing parameters. A constant loading rate of 0.005 mm/s is applied for all the tests. The entire load and displacement histories are measured with linear variable displacement transducers (LVDT) and a 50 kN load cell respectively.

Fig. 1 (a) MTS hydraulic servo-control testing system and (b) split Hopkinson pressure bar (SHPB) system.

Dynamic test is conducted using a 25 mm SHPB system (Fig. 1b). It is composed of a 200 mm striker bar, a 1500 mm incident bar and a 1200 mm transmitted bar, all made of high strength maraging steel. The specimen is sandwiched between the incident and transmitted bars. Two strain gauges are mounted at 733 mm and 655 mm away from the bar-sample interfaces on the incident bar and transmission bar, respectively. An eight-channel Sigma digital oscilloscope by Nicolet is used to record and store the strain signals collected from the Wheatstone bridge circuits after amplification.

The impact of a striker bar on the free end of the incident bar induces a longitudinal compressive wave propagating in both directions. The left-propagating wave is fully released at the free end of the striker bar and forms the trailing end of the incident compressive pulse (Fig. 2). When the leading edge of the compression wave (incident wave) reaches the bar-specimen interface, it is partly reflected (reflected wave), and the remainder passes through the specimen to the transmitted bar (transmitted wave). These three elastic stress pulses in the incident and transmitted bars are recorded with the strain gauges. Assuming one-dimensional stress wave propagation, the forces on both ends of the sample are:

$$P_1 = AE(\varepsilon_i + \varepsilon_r), P_2 = AE\varepsilon_t \tag{1}$$

Here P_1 is the force on the incident end of the specimen, and P_2, the transmitted end. ε denotes strain, and the subscripts i, r and t refer to the incident, reflected and transmitted waves, respectively. A is the cross-sectional area and E denotes the Young's modulus of the bars.

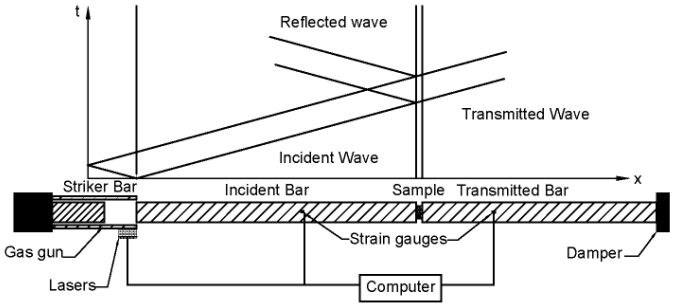

Fig. 2 Schematics of a compression split-Hopkinson pressure bar (SHPB) and the X-t diagram of stress waves.

A newly developed pulse shaping technique of SHPB method is utilized. The pulse shaping technique in SHPB is especially useful for investigating dynamic response of brittle materials such as rocks (Frew et al., 2001, 2002). Without proper pulse shaping, it is difficult to achieve dynamic stress equilibrium in such materials because the sample may fail immediately from its end when it is impacted by the incident bar. In the modified SHPB test, we use the C11000 copper as the main shaper to transform the incident wave from a rectangular shape to a ramped

shape. In addition, a small rubber disc is placed in front of the copper shaper to further reduce the slope of the pulse to a desired value. During tests, the striker impacts the pulse shapers before the incident bar, thus generating a non-dispersive ramp pulse propagating into the incident bar and thus facilitating the dynamic force balance for the SCB specimen (Frew et al., 2001, 2002).

3 METHODOLOGIES

3.1 *SCB sample preparation*

Laurentian granite (LG) is taken from the Laurentian region of Grenville province of the Precambrian Canadian Shield, north of St. Lawrence and north-west of Quebec City, Canada. LG is a fine-grained granitic rock and is considered to be homogeneous and isotropic. The mineral grain size of LG varies from 0.2 to 2 mm with the average quartz grain size of 0.5 mm and the average feldspar grain size of 0.4 mm, with feldspar being the dominant mineral (60%) followed by quartz (33%). Biotite grain size is of the order of 0.3 mm and constitutes 3–5% of this rock. The physical and strength properties of LG are summarized in Table 1.

Table1 Summary of physical and strength properties of Laurentian granite (Iqbal & Mohanty, 2006)

Density	Porosity	Void ratio	Young's modulus	Poisson's ratio	Tensile strength	Compressive strength
1.63 g/cm	0.64%	0.006	92 GPa	0.21	12.8 Mpa	259 MPa

The SCB sample has been developed for tensile strength measurements under quasi-static conditions (Aravani & Ferdowsi, 2006); here this sample configuration is adopted for both static and dynamic tests. Rock cores with a nominal diameter of 40 mm are directly drilled from the rock block. We then slice the rock cores to obtain disk samples with an average thickness of 16 mm. All the disc samples are polished afterwards resulting in surface roughness of less than 0.5% of the sample thickness. The SCB samples are directly made from the BD samples by splitting one BD sample into two halves.

3.2 *Data reduction for static tests*

The SCB method can be viewed as an integration of BD and three-point bend (TPB). Compared with BD, the failure load needed for SCB is much smaller for a given material. Consequently, the stress concentration at the contacts, which may lead to pre-mature failure, is less likely for SCB. Compared with TPB method, SCB specimen is core-based and thus easier to be made for rock cores. In addition, the semi-circular geometry of SCB specimen is easier to be properly aligned than TPB specimen. The loading configuration of the SCB in the MTS hydraulic servo-control testing system is schematically shown in Fig. 3a, where R is the radius of the half disk and B is the thickness of the rock disc. The span between two supporting pins is S. Upon impact, failure will be initiated at the failure spot O on the specimen due to bending.

Using a dimensional argument, the equation for calculating the tensile stress at O is:

$$\sigma(t) = \frac{P(t)}{\pi BR} \cdot Y(S/2R) \tag{2}$$

where $P(t)$ is the time-varying load recorded in the test. The dimensionless stress *Y(S/2R)* is a function of dimensionless distance *S/2R* and can be calibrated using finite element analysis as:

$$Y(S/2R) = \frac{\sigma}{P/\pi BR} \tag{3}$$

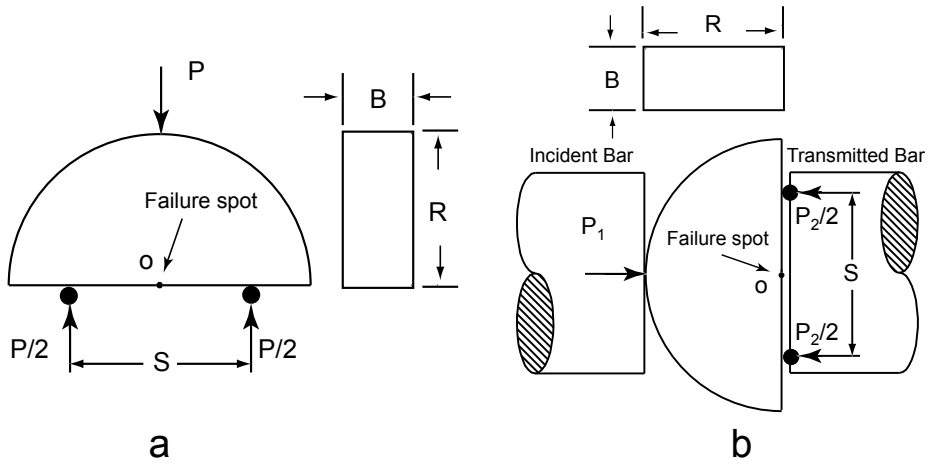

Fig. 3 Schematics of the semi-circular bending (SCB) testing (a) in a MTS machine (b) in a SHPB system.

For the fixed geometry of the SCB sample used in this research (R = 20 mm, B = 16 mm, S = 21.8 mm), Y is equal to 5.14 according to our finite element calibration with ANSYS. The flexural tensile strength is taken as the maximum tensile stress in the history of $\sigma(t)$ and the corresponding loading rate is the slope of the pre-peak linear portion of the $\sigma(t)$ curve.

3.3 *Data reduction for dynamic tests*

The loading configuration of the SCB in the SHPB system is schematically shown in Fig. 3b. The curved end of the specimen is in tangential contact with the incident bar, and the flat end is in contact with the transmitted bar through two supporting pins separated also by the same distance S as in static SCB tests.

To determine the dynamic tensile strength in our proposed SCB test, the quasi-static analysis is employed. We only need to replace the load history used in Eq. (2) with the dynamic load history determined from stress wave analysis (Dai et al., 2008). However, for dynamic tests conducted on SHPB apparatus featuring high loading rates, there is a load inertial effect as shown by Böhme and Kalthoff (Bohme & Kalthoff, 1982). This inertial effect will lead to error in data reduction if we used quasi-static analysis. In our proposed SCB-SHPB method, we showed that with dynamic force balance, the inertial effect can be significantly reduced (Frew et al., 2001, 2002). We demonstrated that in the conventional SHPB tests, the dynamic forces on both ends of the specimen are very different. The resulting inertial effect causes two peaks in the transmitted force pulse, and also a distinct delay of the peak transmitted force with respect to the crack onset. The far-field loading from either incident side or transmitted side cannot reflect the stress state at the failure spot. On the other hand, in a modified SHPB test with proper pulse shaping, the dynamic force balance can be achieved for the entire loading period (i.e., $P_1 = P_2$ in Fig. 3b) and the tensile stress state at the failure spot in the sample can be calculated with quasi-static analysis using the far-field measurements as inputs. Moreover, the rupture time synchronizes with the peak of the transmitted pulse recorded in the SHPB system after corrections for travel time. In this case, the time-varying transmitted force does reflect the loading-bearing capability of the sample, similarly to the quasi-static case. Therefore, the dynamic tensile strength can be confidently calculated from the spike of the transmitted wave assuming quasi-static analysis (Dai et al., 2008).

3.4 *Utilization of new techniques in SHPB*

Pulse shaping technique is employed for the dynamic SCB tests. The dynamic force equilibrium on the two loading ends of the sample is critically assessed. To compare the force histories of

these two, the time zeros of the incident and reflection stress waves are shifted to the sample-incident bar interface and the time zero of the transmitted stress wave is shifted to the sample-transmitted bar interface invoking 1D stress wave theory. Fig. 4 compares the time-varying forces on both ends of the sample for a typical dynamic SCB test. The dynamic forces on both sides of the samples are almost identical before the critical failure point is reached during the dynamic loading. The resulting loads on either side of the sample also feature a linear portion before the peak, thus facilitating a constant loading rate via $\dot{\sigma} = \frac{k}{\pi BR} \cdot Y(S/2R)$. The parameter k in the previous equation is the loading rate as illustrated in Fig. 4.

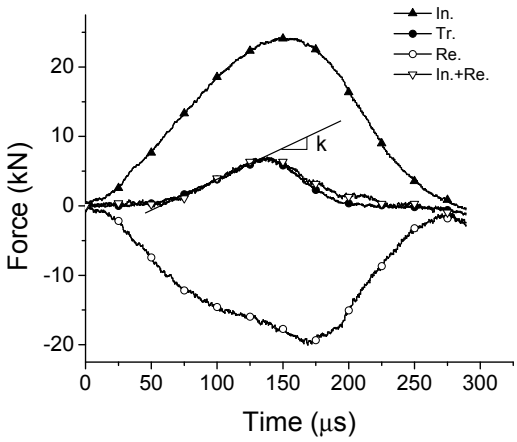

Fig.4 Dynamic force balance check for a typical dynamic SCB test with pulse shaping in SHPB.

3.5 *Numerical simulation of dynamic SCB tests*

To visualize the rock dynamic fracture process of SCB specimen, a combined FEM/DEM method (Y2D code) is utilized to qualitatively simulate our experiments (Munjiza et al., 1999). This numerical method is handy to deal with problems where transition from continuum media to discrete media (e.g., fracture, fragmentation) occurs. Fractures are modeled using a smeared crack approach, with a single crack being replaced by a blunt crack band. Crack opening is then governed by crack face constitutive laws (i.e., strain softening constitutive law or damage mechanics based law).

A dynamic SCB-SHPB test is simulated with Y2D. Plane three nodes triangle element is utilized for the mesh. The recorded loads from the dynamic test are used as inputs to the two platens as boundary conditions (Fig. 6a). The total model is meshed by 3673 elements and 1940 nodes. In the simulation, the Young's modulus of the rock E = 92 GPa and Poisson's ratio ν = 0.21 (Iqbal & Mohanty, 2006). Dynamic tensile strength σ_t is taken as 33.8 MPa, determined from our testing result and fracture energy G_f is 0.05 N/mm. The material properties of the two platens are chosen the same as the bars in the SHPB test, with Young's modulus of 200 GPa and Poisson's ratio of 0.29.

Fig.5b illustrates the macroscopic crack initiation from the centre of the sample's diameter, where the generated tensile stress is the maximum. From Fig. 5c to Fig. 5e, the macroscopic crack propagates to the incident bar end of the sample along the loading axis, resulting in the final catastrophic failure of the SCB sample in Fig.5e. The fracture pattern of the recovered SCB sample for this test is shown in Fig.5f. Good agreement has been reached between the simulated fracture pattern and experimental observation. This shows that the primary failure of the SCB test is tensile and the failure indeed started from the failure spot *O*, where the tensile stress is the largest.

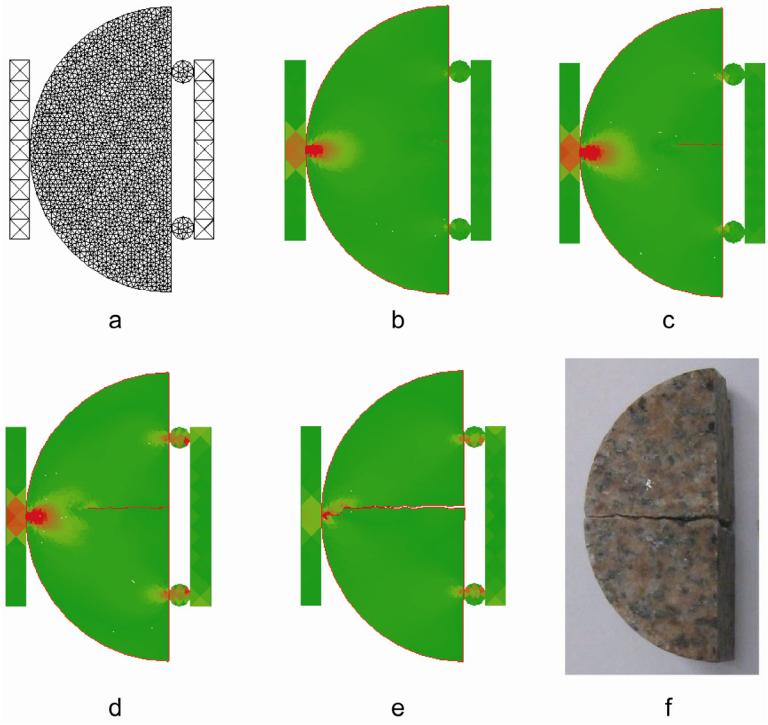

Fig. 5 FEM/DEM simulation of a dynamic SCB test.
(a) FEM/DEM model in Y2D, (b) to (e) representative snap-shots of the fracture process and (f) the re-covered SCB sample.

4 RESULTS

4.1 *Experimental results*

The static and dynamic flexural tensile strengths obtained from our SCB tests are tabulated in Table 2. The static flexural tensile strength is averaged from four tests. The measured strengths feature strong rate dependence. The maximum measured dynamic tensile strength is 85.8 MPa with the loading rate of 2380 GPa/s, which is 3.2 times higher than the static tensile strength of 26.2 MPa with a very low loading rate of 0.2.6 MPa/s.

Table 2 Experimental results of static and dynamic SCB tests

Loading Rate (GPa/s)	Flexural Tensile Strength (MPa)	Non-local Correction (MPa)
2.60E-04	26.2	14.6
373	33	18.3
378.3	33.8	18.7
429	38.5	21.4
449	37.4	20.8
468	36.3	20.2
569	36.4	20.2
675	41.3	22.9
1030	52.3	29.1
1070	54.7	30.4
1230	62.8	34.9
1300	66.5	36.9
1450	52.7	29.3
1510	57.8	32.1
1900	75	41.7
2380	85.8	47.7
2610	80.5	44.7

The results are also illustrated in Fig. 6, accompanied by the tensile strength measured from dynamic BD test (Iqbal et al., 2008) for comparison purpose. Overall, the measured strengths of LG exhibit a linear increase with the loading rates. Linear fit of the dynamic strengths from SCB tests and BD test result in Eq. (4) and Eq. (5) are:

$$\sigma_f = 0.0234\dot{\sigma} + 26.7 \tag{4}$$

$$\sigma_t = 0.0125\dot{\sigma} + 17.9 \tag{5}$$

where σ_f is the flexural strength and σ_t is the tensile strength. This rate dependence of tensile strength of rocks has long been identified in the literature and the mechanism of causing it has also been discussed (Grady & Kipp, 1980; Zhao & Li, 2000). Grady and Kip (Grady & Kipp, 1980) attribute the rate effects to the interaction of micro-cracks in rocks. In the static tests, the principle crack or the critical crack will develop and contribute to the breakage of the sample; while in the dynamic tests, micro-cracks will interact before a principle crack is formed.

The flexural strength measured with the SCB method is higher than the tensile strength measured with BD method for a given loading rate. This phenomenon has been observed in the static tensile measurements with a stress gradient around the potential failure spot (Coviello et al., 2005; Hudson et al., 1972; Lajtai, 1972; Mellor & Hawkes, 1971). In the tensile property measurement of a granite under intermediate loading rates, Zhao and Li (Zhao & Li, 2000) also reported the higher value of dynamic strength from their 3-point flexural test as compared to that obtained by BD test. No quantitative interpretation has been made for this discrepancy.

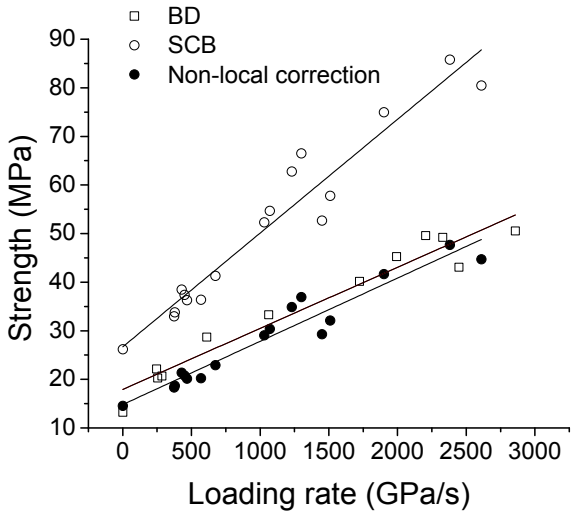

Fig.6 Comparison of strengths from dynamic SCB test and BD test (Iqbal et al., 2008) as well as the reconciliation by non-local failure model.

4.2 *Reconciliation of flexural tensile strength with tensile strength*

A non-local approach (Carter, 1992; Lajtai, 1972; Van de Steen & Vervoort, 2001) is utilized here to reconcile the discrepancy of measured dynamic results from SCB and BD tests. Since the dynamic equilibrium is ensured for all SCB tests, the non-local approach should work for our dynamic tests. This theory states that the material fails when the local stress averaged over a distance δ along the prospective fracture path reaches the tensile strength σ_t (Van de Steen & Vervoort, 2001):

$$\sigma_t \delta = \int_{l_0}^{l_0+\delta} \sigma \, dl \tag{6}$$

where δ is designated as an characteristic material length scale and σ is the distribution of the tensile stress over δ. Numerical method is used here to determine σ_t for a given sample geometry. Here we assume $\delta = 6mm$, as suggested for rocks (Van de Steen & Vervoort, 2001). The tensile stress gradient along the prospective fracture path of our SCB sample is calculated numerically with finite element analysis, as shown in Fig. 7. Polynomial fit of the normalized stress gradient results in the following equation:

$$\frac{\sigma}{\sigma_m} = 0.01277x^2 - 0.2028x + 0.99832 \tag{7}$$

where σ is the tensile stress along the prospective fracture path, σ_m is the tensile stress at the failure spot (also the maximum tensile stress in the sample), x is the distance of a point along the fracture path to the centre of the SCB sample (see the insert in Fig. 7). Substituting Eq.(7) to Eq. (6), the relationship between flexural tensile strength σ_f and the resulting tensile strength σ_t is determined as $\sigma_f / \sigma_t = 1.8410$.

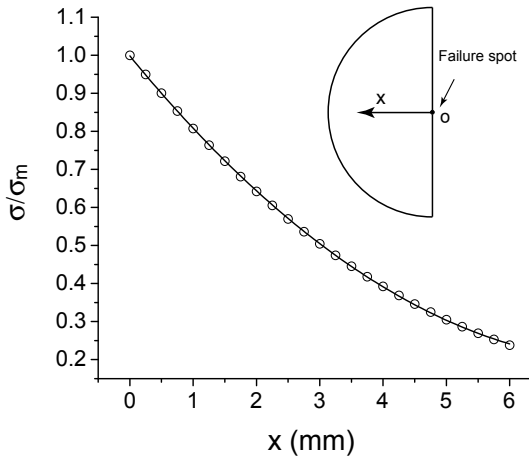

Fig.7 Normalized tensile stress along the prospective fracture path in SCB sample; x is the distance of a point along the prospective fracture path to the failure spot of the SCB sample (see the insert).

Employing non-local failure theory, the actual tensile strength can be deduced from the measured static or dynamic maximum flexural strength σ_f at failure. The results are also included in Fig. 7. Overall, the corrected tensile strengths from flexural strength agree well with those measured from BD tests. Specifically, the adjusted static tensile strength from SCB test is determined to be 14.6 MPa, which is very close to the measured results of 12.8 MPa from BD tests. The corrected tensile strengths are also linearly fitted with Eq. (8) shown in Fig. 7.

$$\sigma_t = 0.013\dot{\sigma} + 14.8 \tag{8}$$

5 CONCLUSION

We measured flexural tensile strength of LG with a newly proposed semi-circular bend method statically using a MTS hydraulic servo-control testing and dynamically using a split Hopkinson pressure bar system. A numerical code (Y2D) using FEM/DEM coupled method is utilized to visualize the fracture process of dynamic SCB test and the results validate the tensile nature of the failure. With proper pulse shaping, dynamic far-field force balance is achieved and quasi-static analysis is thus valid for deducing the flexural tensile strength from the SHPB measurements. The flexural tensile strength of LG exhibit strong rate dependence, an almost linear increase with measured loading rates ranging from ~0 GPa/s to ~ 3000 GPa/s. The flexural tensile strength measured from SCB test has a higher value than that the tensile strength measured us-

ing BD method under similar loading rates. We rationalize this discrepancy using a non-local failure theory.

ACKNOWLEDGEMENTS

The authors acknowledge the financial support by NSERC/ Discovery Grant No.72031326.
Y2D code is developed by Prof. Monjiza from Queen Mary University of London.

REFERENCES

Aravani, M., & Ferdowsi, B., 2006, Evaluating the semi-circular bend test as a new method to determine tensile strength of asphalt concrete mixture: *7th International Congress on Civil Engineering*.

Bieniawski, Z. T., & Hawkes, I., 1978, Suggested methods for determining tensile strength of rock materials: *International Journal of Rock Mechanics and Mining Sciences*, v. 15, p. 99-103.

Bohme, W., & Kalthoff, J. F., 1982, The behavior of notched bend specimens in impact testing: *International Journal of Fracture*, v. 20, p. R139-R143.

Cai, M., Kaiser, P. K., Suorineni, F., & Su, K., 2007, A study on the dynamic behavior of the Meuse/Haute-Marne argillite: *Physics and Chemistry of the Earth*, v. 32, p. 907-916.

Carter, B. J., 1992, Size and stress gradient effects on fracture around cavities: *Rock Mechanics and Rock Engineering*, v. 25, p. 167-186.

Coviello, A., Lagioia, R., & Nova, R., 2005, On the measurement of the tensile strength of soft rocks: *Rock Mechanics and Rock Engineering*, v. 38, p. 251-273.

Dai, F., Xia, K. W., & Luo, S. N., 2008, Semi-circular bend testing with split Hopkinson pressure bar for measuring dynamic tensile strength of brittle solids: *Review of Scientific Instruments*, v. 79.

Frew, D. J., Forrestal, M. J., & Chen, W., 2001, A split Hopkinson pressure bar technique to determine compressive stress-strain data for rock materials: *Experimental Mechanics*, v. 41, p. 40-46.

Frew, D. J., Forrestal, M. J., & Chen, W., 2002, Pulse shaping techniques for testing brittle materials with a split Hopkinson pressure bar: *Experimental Mechanics*, v. 42, p. 93-106.

Goldsmith, W., Sackman, J. L., & Ewert, C., 1976, Static and dynamic fracture strength of barre granite: *International Journal of Rock Mechanics and Mining Sciences*, v. 13, p. 303-309.

Grady, D. E., & Kipp, M. E., 1980, Continuum modeling of explosive fracture in oil-shale: *International Journal of Rock Mechanics and Mining Sciences*, v. 17, p. 147-157.

Hudson, J. A., 1969, Tensile strength and ring test: *International Journal of Rock Mechanics and Mining Sciences*, v. 6, p. 91-97.

Hudson, J. A., Rummel, F., & Brown, E. T., 1972, The controlled failure of rock disks and rings loaded in diametral compression: *International Journal of Rock Mechanics and Mining Sciences*, v. 9, p. 241-248.

Iqbal, M. J., Mohanty, B., & Xia, K., 2008, Dynamic tensile strength and mode-I fracture toughness in granitic rocks: *Proceedings of the XIth International Congress and Exposition, Orlando, Florida, USA*.

Iqbal, N., & Mohanty, B., 2006, Experimental calibration of stress intensity factors of the ISRM suggested cracked chevron-notched Brazilian disc specimen used for determination of mode-I fracture toughness: *International Journal of Rock Mechanics and Mining Sciences*, v. 43, p. 1270-1276.

Lajtai, E. Z., 1972, Effect of tensile stress gradient on brittle-fracture initiation: *International Journal of Rock Mechanics and Mining Sciences*, v. 9, p. 569-578.

Mellor, M., & Hawkes, I., 1971, Measurement of tensile strength by diametral compression of discs and annuli: *Engineering Geology*, v. 5, p. 173-225.

Munjiza, A., Andrews, K. R. F., & White, J. K., 1999, Combined single and smeared crack model in combined finite-discrete element analysis: *International Journal for Numerical Methods in Engineering*, v. 44, p. 41-57.

Ravichandran, G., & Subhash, G., 1994, Critical appraisal of limiting strain rates for compression testing of ceramics in a split Hopkinson pressure bar: *Journal of the American Ceramic Society*, v. 77, p. 263-267.

Van de Steen, B., & Vervoort, A., 2001, Non-local stress approach to fracture initiation in laboratory experiments with a tensile stress gradient: *Mechanics of Materials*, v. 33, p. 729-740.

Wang, Q. Z., Li, W., & Song, X. L., 2006, A method for testing dynamic tensile strength and elastic modulus of rock materials using SHPB: *Pure and Applied Geophysics*, v. 163, p. 1091–1100.

Zhao, J., & Li, H. B., 2000, Experimental determination of dynamic tensile properties of a granite: *International Journal of Rock Mechanics and Mining Sciences*, v. 37, p. 861-866.